Establishing a Bayesian Approach to Determining Cosmogenic Nuclide Reference Production Rates Using He-3

Brent M Goehring[1^], Paul Muzikar[2], Nathaniel A Lifton [2,3]

[1] Department of Earth and Environmental Sciences, Tulane University, New Orleans, LA

[2] Department of Physics, Purdue University, West Lafayette, IN

[3] Department of Earth, Atmospheric, and Planetary Sciences, Purdue University, West Lafayette, IN

^Corresponding Author

Keywords: cosmogenic nuclide, helium-3, production rate, calibration, Bayesian, erosion

Abstract

Production rates are a cornerstone of in situ cosmogenic nuclide applications, including surface exposure dating, erosion rate/denudation rate estimates, and burial dating. The most common approach for estimating production rates is to measure cosmogenic nuclide samples from sites with independently well-constrained exposure histories. In addition, while researchers attempt to minimize the effects of erosion through careful site and sample selection, it can be present at some unknown level in certain sites. We present a general Bayesian methodology for combining information from the nuclide concentrations, the exposure history, and the possibility of erosion, to determine the production rate at a given site. Then, we use another Bayesian approach to combine the results from the various sites.

Cosmogenic ^{3}He is an ideal test-bed for our Bayesian approach. It has the most calibration sites of the commonly measured cosmogenic nuclides, and there is evidence for the effect of erosion on some of the sites. Our approach largely reconciles previous discrepancies between sites of widely varying age, even at latitudes where geomagnetic effects are significant. With the canonical Lal/Stone scaling scheme, we derive a global sea level high latitude ^{3}He production rate of 118±2 atoms g^{-1} yr^{-1} when considering olivine and pyroxene together. Using the Lifton-Sato-Dunai scaling scheme yields a similar rate of 121±2 atoms g^{-1} yr^{-1}. Uncertainties

associated with these values are improved over previous studies, due to both reduced scatter among the sites and an approach to combining sites which deemphasizes outliers.

1. Introduction

Cosmogenic nuclide production rates are most commonly derived empirically from locations with well-constrained exposure histories. In this context, ‘well-constrained’ generally refers to good independent age control, but also includes inferences regarding geomorphic history (e.g., surface erosion, uplift, and/or ash and sediment cover). The method by which the independent exposure age is estimated varies; in general, most researchers have taken the well-reasoned and simple approach of choosing an exposure age thought to represent the central tendency of the data constraining the sites exposure age and assumed Gaussian uncertainties on the age (Borchers et al., 2016). Information regarding the geomorphic history of a site tends to be more subjective and more difficult to quantify. For that reason, most cosmogenic nuclide calibration sites tend to be from surfaces impacted by geologically instantaneous events. Quantification of the long-term erosion of a calibration site surface is less-well-understood, but generally is derived from the measurement of differential surface relief or preservation of fine surface features or patinas. However, in many studies erosion is assumed to be small enough in magnitude to be ignored and assumed equal to zero.

Cosmogenic helium-3 (^{3}He) was among the first cosmogenic nuclides to be studied in detail (e.g., Cerling, 1990; Kurz, 1986; Kurz et al., 1990) and as such many production rate calibration sites exist. Published ^{3}He production rate calibration sites span a wide-range of ages (ca. 2 - 1350 ka), latitudes (ca. 50°S to 66°N), and elevations (ca. 0 to 4000 m). While most studies yield sea level high latitude ^{3}He production rates near 120 atoms g^{-1} yr^{-1}, some yield significantly higher production rates and others anomalously low reference production rates. Following Goehring et al. (2010) a reference ^{3}He production rate refers to the rate of ^{3}He production at sea level and high latitude via scaling of the site production rate to sea level and high latitude. Figure 1 shows the distribution of reference ^{3}He production rates for the sites used in our analysis relative to scaling of Lifton et al. (2014) and time-dependent geomagnetic and atmospheric frameworks presented in Lifton (2016). No apparent trends ($r^2 < 0.1$) are observed between the production rate and age, site latitude or site elevation. To first order this suggests that there are no systematic temporal or spatial biases contained within the geomorphic and scaling models used to derive reference ^{3}He production rates. Yet, several ^{3}He calibration studies have reference production rates that are lower than canonical values even when all studies are scaled using the same parameters and models (e.g., Dunai and Wijbrans, 2000; Fenton et al., 2013; Foeken et al., 2012). The observation of a handful of anomalously low ^{3}He reference production rates raises three possibilities. First, it is possible that temporal variations in the Earth's geomagnetic field (and hence cosmogenic nuclide production) are not adequately described by geomagnetic field reconstructions used in the current scaling models for the handful of specific sites; however, one would expect the appearance of trends more robust than presently observed if this were the case. Second, factors such as laboratory biases might have an influence (Blard et al., 2014), as measurements of cosmogenic ^{3}He are made in several different laboratories using differing procedures and standardizations, and could lead to anomalously low values. Finally, lower reference production rates can result for young flows due to temporary ash or other sediment cover that was later eroded, or from underestimating surface erosion magnitude at a site (Figure 2). The former scenario is more important for young flows, where a significant portion of the integrated exposure history may have occurred with ash or sediment cover. Considering the absence of any significant spatial or temporal trends in Figure 1 when reference production rates are calculated using internally consistent scaling systematics and the coefficient of variation due to laboratory biases is smaller than differences in calibrated production rates, we focus our analysis on erosion below.

Here we formalize a Bayesian approach to cosmogenic nuclide production rate calibration, explicitly accounting for uncertainties associated with calibration site erosion characterization. Additionally, our Bayesian approach also allows for non-Gaussian site age probability distributions, much like that of Borchers et al. (2016). The methods presented here can be generalized and applied to the other in situ cosmogenic nuclides. Finally, we present a global reference ^{3}He production rate with lower overall uncertainties than other published compilations because of reduced scatter in the ^{3}He production rate calibration dataset when potential erosion is accounted for. Thus, we are making use of Bayesian thinking in two separate parts of this paper; first, in the development following Equation 1, and second, in the development following Equation 9.

2. Calibration Datasets

There are five recent ^{3}He production rate compilations, Goehring et al. (2010), Borchers et al. (2016), Lifton (2016), Delunel et al. (2016), and Martin et al. (2017). The five datasets have many similarities in terms of the sites included in their compilations, with the Borchers et al. (2016), Lifton (2016), Delunel et al. (2016), and Martin et al. (2017) compilations incorporating calibration studies published since 2010, while omitting some of the studies included in Goehring et al. (2010). Exclusion of sites in the Borchers et al. (2016) study followed the criteria outlined by the CRONUS-Earth project for primary and secondary calibration sites, while the Delunel et al. (2016) and Martin et al. (2017) studies were more ad hoc in their exclusions. Since the Borchers et al. (2016) compilation data was finalized for calculation, additional calibration studies have been published from Bolivia (Blard et al., 2013), the island of Fogo (Foeken et al., 2012), Arizona (Fenton et al., 2011; Fenton et al., 2013), New Zealand (Eaves et al., 2015), and Argentina (Delunel et al., 2016). The complete list of calibration datasets used here is summarized in Table S1. In this study, we take a more inclusive approach and consider each site to have equal weight and therefore do not separate into primary and secondary sites and include all previously published ^{3}He production rate data.

3. Methods

Before proceeding further, we define what we mean by a "site". Some previous compilations have grouped individual calibration sites by geographic proximity and/or age (e.g., Goehring et al., 2010). In this work, a "site" refers to a calibration site as defined first by its age, and second by its geographic location. For example, there may be multiple sites with similar and/or related ages (e.g., Tabernacle Hill and the Lake Bonneville Flood deposits) that are in distinctly different geographic locations; each geographic location is treated as a separate site. Alternatively, there can be multiple calibration sites with different ages within a relatively confined geographic region (e.g., Hawaii); again, we treat each as a separate site. Our definition of a site thus helps us set up our analysis and contrasts with previous approaches, where chi-square minimizations of samples from a region have generally been treated as a single dataset (e.g., Balco et al., 2009), and the best-fitting reference production rate determined by minimizing the misfit between the measured and predicted ages or concentrations given.

3.1 Mathematical Framework

Rather than using a chi-squared minimization to derive a best-fitting reference production rate, we adopt a Bayesian approach to determine the reference production rate posterior probability distribution for each site. A distinct advantage of the Bayesian approach is the ability to incorporate additional information in the form of prior probability distributions of both the site independent age and surface erosion history that are not incorporated into previous approaches (e.g., Balco et al., 2009; Goehring et al., 2010).

Following Bayes theorem, we can state that

$$f(P,t,\varepsilon \mid \mu) f(\mu) = f(\mu \mid P,t,\varepsilon) f_0(P,t,\varepsilon) \quad (1)$$

which relates what we want, the probability density functions for the production rate P, site age t, and site erosion rate ε, given the ^{3}He concentration μ we measure, to what can be readily computed, namely the probability of observing the measured data given P, t, and ε. In the formulation considered here, μ is the set of ^{3}He concentrations at a site, f(μ) is the prior probability of observing the data (which does not need to be specified if we are willing to normalize the results at the end of the calculations), and f_0(P,t, ε) are the prior probability constraints on P, t, and ε. Therefore, we can write

$$f(P,t,\varepsilon \mid \mu) = c f(\mu \mid P,t,\varepsilon) f_0(P,t,\varepsilon) \quad (2)$$

where *c* is chosen such that

$$\iiint f(P,t,\varepsilon \mid \mu) \, dP \, dt \, d\varepsilon = 1 \quad (3).$$

An expression for f(μ|P,t, ε), or the likelihood of observing a ^{3}He concentration (μ) for sample *i* at a site given a range of P, t, and ε, is

$$f(\mu \mid P,t,\varepsilon) = \prod_i e^{\frac{(\mu_i - \phi_i(P,t,\varepsilon))^2}{2\sigma_\mu^2}} \quad (4)$$

The term ϕ(P,t, ε) is the ^{3}He concentration predicted using the standard equation describing the buildup of a stable cosmogenic nuclide in a steadily eroding surface (Lal, 1991, Eqn. 6). The predicted concentration and associated Gaussian analytical measurement uncertainty ($\sigma_{\mu i}$) for each sample describe a Gaussian function. The likelihood at a site is represented by the product of the Gaussians over all samples at a site. The joint probability distribution for P, t, and ε at a site is therefore described by

$$f\left(P,t,\varepsilon \mid \mu\right) = c\left(\prod_i e^{\frac{\left(\mu_i - \phi_i\left(P,t,\varepsilon\right)\right)^2}{2\sigma_\mu^2}}\right) f_0\left(P,t,\varepsilon\right) \quad (5).$$

The prior contains information regarding knowledge of the ^3He production rate, independent age of the site, and surface erosion history, which is uniform for all samples in the study here. We argue this provides for a more robust production rate determination.

The probability distribution for P is then

$$f\left(P\right) = \iint f\left(P,t,\varepsilon \mid \mu\right) dt\, d\varepsilon \quad (6),$$

and we can calculate the average production rate and its uncertainty from

$$\begin{aligned} \langle P \rangle &= \int f\left(P\right) dP \\ \sigma^2 &= \int f\left(P\right) \bullet \left(P - \langle P \rangle\right)^2 dP \end{aligned} \quad (7 \text{ and } 8).$$

The definitions of the prior probabilities for the parameters of interest are of critical importance when employing a Bayesian approach. In our case, these are the ^3He reference production rate at sea level and high latitude (SLHL), the independent age of the site of interest, and the probability distribution for erosion of sample surfaces. We employ a uniform probability distribution for the SLHL production rate between 50 and 250 atoms g^{-1} yr^{-1} for all sites.

The prior probability for the independent age of the calibration sites considered here, unlike the prior for the ^{3}He reference production rate and surface erosion, the uniqueness of each site necessitates different prior probabilities for each site. We take three approaches here. For sites such as volcanic lava flows directly dated by radiometric methods such as K-Ar or ^{40}Ar/^{39}Ar we use the reported value and one-sigma standard deviation and assume Gaussian probability (e.g., Fenton et al., 2011; Fenton et al., 2013). A second group of sites is either dated via radiocarbon methods, such as radiocarbon dating of charcoal left behind in tree molds (e.g., Licciardi et al., 1999), or a combination of radiocarbon and U-series dating methods on deposits that provide minimum and maximum limiting ages (e.g., Goehring et al., 2010). In the former case, we have combined the ages following standard practices for combining multiple radiocarbon ages either directly dating an event or bracketing an event to produce a probability distribution for the site age (Bronk Ramsey, 2001). In the latter, we follow methods such as those outlined in Kelly et al. (2015) and Blard et al. (2013) to produce a probability distribution for the calibration site based on the probability distributions for the minimum and maximum limiting deposits. Finally, sites associated with the catastrophic draining of pluvial Lake Bonneville (Amidon and Farley, 2011; Cerling and Craig, 1994; Goehring et al., 2010) are assumed to have a uniform probability distribution between conservative bounds of the age of the Bonneville flood using a combination of radiocarbon and U-series techniques in various settings (e.g., Benson et al., 1990; McGee et al., 2012; Oviatt et al., 1992; Oviatt and Nash, 1989).

The prior probability distribution for erosion is harder to define, as the general approach has been to assume either no erosion of sampled surfaces, or if evidence in the form of differential erosion is present, to assume a fixed erosion for all samples at a site. Portenga et al. (2011) compiled a global dataset of ^{10}Be-derived basin scale (n=1149) and maximum limiting outcrop (n=450) erosion rates. We fit an exponential distribution to their outcrop dataset to use as the prior in our analysis; for reference, the resulting mean is equal to 7.76 m Myr^{-1}, and use this probability distribution as the prior for surface erosion in our study. One note of caution is that the Portenga et al. (2011) dataset is largely based on the measurement of erosion rates in felsic rocks, whereas the vast majority of sites in the present study are from mafic rocks and thus there are likely differences in the weathering characteristics of the two igneous rock compositions. Given that a calibration site should have a well-constrained exposure history, and is typically chosen to minimize erosion effects, we limit erosion rates in this study to a low range of 0 to 5 m Myr^{-1} with probabilities for this range of erosion rates drawn from the exponential distribution fit to the Portenga et al. (2011) outcrop dataset. Furthermore, we limit the range of erosion rates considered at a given site to those less than that resulting in 1 m of total erosion over the exposure history.

Using the methods outlined above, our Bayesian approach results in a probability distribution for the reference ^{3}He production rate derived from the data and characteristics of each site. We believe this approach provides an advantage over previous ones in that the structure of the resulting posterior probability distribution yields information about a site's reliability as a production rate calibration site (e.g., strongly affected by sample scatter or strongly influenced by erosion).

3.2 Determination of a Global Production Rate

We now turn to the task of combining the results from all of the sites into an optimal global reference production rate and note that the approach discussed below is also applicable to the development of regional production rates. The estimation of a single reference "global" production rate for a cosmogenic nuclide provides a simple basis for applications using that nuclide, and provides a convenient means for comparing production rate compilations such as that presented here with previous efforts. This traditionally has been done using common statistical methods (e.g., mean and median). Muzikar et al. (2017) review an elegant approach developed by Press (1997) that provides an objective way to allow for the fact that results from some sites may be inconsistent with the rest. The attractiveness of this technique stems from the inclusion of all sites, with an equal likelihood of being part of a consistent whole, yet any inconsistencies are objectively deemphasized in the resulting distribution.

To implement, we take the posterior distribution generated for each site and calculate average (P_j) and standard deviation (σ_j) following Eqs. 7 and 8 and assume a Gaussian distribution. Following Press, we then assume that for each site, there is a probability β (with β between zero and one) that this result is consistent with the data, and a probability 1- β that it is inconsistent. At this point we do not know the value of β. We use the data to generate a joint probability distribution for P and β.

The key equation we then use is another version of Bayes' theorem:

$$f(P,\beta \mid results) f(results) = f(results \mid P,\beta) f(P,\beta) \qquad (9)$$

Here, f(P, β |results) is what we want, the joint probability distribution for P and β, given the results from the various sites. Our results are the set (P_j, σ_j). The pdf f(results) is the probability of acquiring the results; similar to Eqs. 1 and 2 it may be omitted if we properly normalize our answer:

$$f(P,\beta \mid results) = cf(results \mid P,\beta) f(P,\beta) \qquad (10)$$

Here, c is a normalization constant chosen to enforce

$$\int_0^\infty dP \int_0^1 d\beta f(P,\beta \mid results) = 1 \qquad (11)$$

The key input comes in modeling the function f(results | P, β), which is the pdf for obtaining our results, given P and β. Again, following Press (1997), we write it as follows:

$$f(results \mid P,\beta)=\prod_{j=1}^{N}\left(\beta G_{\sigma_j}(P_j-P)+(1-\beta)G_s(P_j-P)\right) \qquad (12)$$

Here, we use the following notation for our Gaussians:

$$G_\sigma(x)=\frac{1}{\sqrt{2\pi\sigma^2}}\exp(-\frac{x^2}{2\sigma^2}) \qquad (13)$$

Thus, for each site, we ask, what is the probability of finding result P_j. If the site has a consistent result (probability β) this is given by the Gaussian centered on P, with standard deviation σ_j. If the site is inconsistent (probability 1- β) then it is given by a Gaussian also centered on P, but with a very large standard deviation given by s instead of σ, and thus the two are interchangeable depending on the purpose of the Gaussian. The large value of s produces a very wide Gaussian, which says that an inconsistent site gives us little information as to the true value of P.

Finally, the pdf *f(P, β)* is the prior for this problem; it embodies the probabilities we assign to P and β before we acquired the data. Here we adopt a conservative approach and assign uniform probability to all values of P (0-250 atoms g^{-1} yr^{-1} and 0-1, respectively). One technical point should be mentioned. The allowed values of P are all positive; so, if one of the Gaussians has statistical weight below zero, we must adjust its normalization factor to account for this using the approach outlined in Muzikar et al. (2017; Eqs. 11 and 12).

The way equation (12) works is as follows. As a given site's deviation from a 'consensus' value based on the other sites increases, the "inconsistent Gaussian" for a deviant site in equation

(12) will tend to have more statistical weight in the final answer than the “consistent Gaussian.” The rate at which the “inconsistent” Gaussian asserts itself with increasing deviation depends on the value of s. However, this broad “inconsistent Gaussian” will tend to not shift the final prediction for P very much towards the prediction of the inconsistent site.

3.3 Cosmic Ray Scaling

For the analysis presented here, we adopt code based on Balco et al. (2008) and Lifton et al. (2014), underlying the CRONUS-Earth Calculator (Marrero et al., 2016; Phillips et al., 2016a; Phillips et al., 2016b). Spatial variation in atmospheric pressure and solar modulation effects follows Lifton et al. (2014). Cosmogenic nuclide scaling in the code uses two approaches: 1) the method outlined in Lal (1991) and modified by Stone (2000), which scales time-invariant total cosmic ray flux for the effects of the dipolar geomagnetic field and atmospheric pressure only, and 2) the nuclide-specific method of Lifton et al. (2014) which scales predicted nuclide production by neutrons, protons, and muons for a given nuclide at a location of interest, accounting for temporal and spatial variations in the geomagnetic field and solar modulation, relative to predicted nuclide SLHL production. Nuclide production in the Lifton et al. (2014) model is predicted by integrating the particle flux at a given site, over a given time period, with the probability of production as a function of energy (the excitation function). Critical to the Lifton et al. (2014) model is the choice of geomagnetic field model (dipolar vs higher-order) and paleomagnetic record. We adopt here the Pavon-Carrasco et al. (2014) time-varying dipolar geomagnetic field as outlined in Lifton (2016).

4. Results

The posterior distribution for each calibration site with and without erosion (Supplementary Figures 1 and 2), along with its average and standard deviation were determined for the 49 ^{3}He production rate calibration sites listed in Table S1. As an example, Figure 3 shows the resulting posterior distributions for three sites that are influenced by different priors with respect to the absolute independent age as well as differing methodological constraints on the age itself that influence the form of the prior (e.g., uniform probability for min-max age constraints, Gaussian probability for Ar-Ar ages, calibrated radiocarbon age probability). Additionally, the sites span a range of ages and therefore may be affected to differing degrees by erosion. Specifically, the examples shown in Figure 3 display the effects of sites with minimum and maximum limiting age constraints, which result in an age prior represented by a uniform distribution (Tabernacle Hill), radiocarbon ages directly dating the calibration site (Yapoah Crater), whose prior incorporates the calibrated radiocarbon age probability distribution, and finally the effects of assuming a Gaussian probability distribution for a site dated by Ar/Ar chronology (SP Flow). The effects of incorporating a probability distribution for the site erosion rate are discussed further below, but in summary the youngest site (Yapoah Crater, ca. 2 ka) shown in Figure 3 shows little effect of incorporating erosion, while the oldest site (SP Flow, ~72 ka) displays a broader probability distribution extending towards higher production rates, particularly relative to the posterior distribution when erosion is neglected. Posterior distributions for every site, both for the case of zero erosion and assuming an exponential distribution for erosion are shown in the Supplementary Material.

Results for the reference global sea level high latitude ^{3}He production rate, including erosion, are summarized in Table 1 using multiple summary statistic approaches, including the Press approach described above, the mean and standard deviation, inverse-error-weighted mean and error-weighted variance, and finally the median and half interquartile range. The resulting probability distributions from the Press approach are shown in Figure 4. For both Table 1 and Figure 4, results are separated by mineral phase. At face value, our results indicate that pyroxene production rates are higher than for olivine; however, at 2σ the differences are not significant and the number of calibration sites for pyroxene is far fewer than for olivine and so we caution over interpretation of our mineral specific results. Additionally, we observe a small peak in the probability of pyroxene production slightly less than 130 atoms g^{-1} yr^{-1} – demonstrating the utility of PDFs in this approach,

As outlined above, use of the Press approach requires assigning a value, s, for the standard error of an “inconsistent” measurement. To avoid unduly biasing results with this approach, selection of s must be balanced so that it is representative of an “inconsistent” Gaussian while not overly influencing the ultimate value for the global reference production rate. Figure 5 shows a sensitivity analysis of our reference production rate with this dataset to different values of s and indicates that for values greater than 20 atoms g^{-1} yr^{-1}, the resulting average production rate is constant over a wide range of values for s. For the results summarized in Table 1 and Figure 4, s has been chosen as five times the mean of the uncertainties for calibration sites; the value for s is generally greater than 50. This is a very conservative application of the Press (1997) approach that therefore tends to not “de-weight” any calibration site based on its uncertainty and rather “de-weights” a site given its deviation from the consensus value. For all the results presented above, similar values are reported for the zero-erosion case in the Supplementary Material S2.

5. Discussion

Erosion acts to remove cosmogenic nuclides from surficial materials; as such, concentrations will be lower in an eroding surface than for a surface experiencing zero erosion (e.g., Lal, 1991). While all sites will be affected to some degree, only the oldest sites will be significantly influenced by incorporating erosion (Figure 2), whether as a fixed value (e.g., Kelly et al., 2015; Phillips et al., 2016a) or in the form of a prior distribution. As shown in Figure 3, the youngest site, Yapoah Flow, shows essentially no influence from our assumed range of surface erosion rates, while the SP Flow displays a widening of the ^{3}He production rate probability distribution to higher values because of its ~72 ka age. The Tabernacle Hill flow displays intermediate influence by erosion in our model. The exponential distribution assumed as the prior for erosion yields higher probabilities for low erosion rates that are more likely than high erosion rates, up to a total of 1 m total erosion. Predicted site production rates not only increase because of erosion effects, but the resulting posterior distribution for ^{3}He production is dependent on the form of the prior for erosion and the independent site age (see below).

In addition to the influence of the prior for erosion, incorporating a prior on the independent age control affects the posterior distribution for ^{3}He production rates. The effect is most notable for sites where independent age control shows some degree of non-Gaussian or non-uniform behavior (e.g., radiocarbon ages with complex calibrated age distributions). We can again turn to the Yapoah Flow shown in Figure 3 as an example. The posterior distribution for this flow shows peaks in probability that reflect peaks in the probability associated with the age prior. Curiously, age constraints for Tabernacle Hill are simple minimum- and maximum-limiting ages and thus the prior distribution is the product of two Heaviside functions. Due to the uniformity of this prior, the strong Gaussian character of the distribution of ^{3}He concentrations in the measured samples, yields a posterior distribution that is nearly Gaussian as well (Figure 3).

As discussed above, the use of the Press method compared to more traditional means of data combination yields useful information beyond just a central tendency and uncertainty. One such measure is the probability of a site being “consistent”. Here, “consistent” simply means compatible with the Press-derived average value for all the sites while simultaneously considering the uncertainty associated with a site. For example, a site with very small uncertainties, but far from the average value, would have a low probability of being “consistent”, compared to a site near the bulk of the data, but with larger uncertainties. In other words, the Press method rewards sites close to the central tendency regardless of uncertainty, and likely explains the similarity of the Press derived average and median values for the global data sets (121 vs 122 atoms g^{-1} yr^{-1}, respectively; LSDn scaling; Table 1). Keeping all other parameters the same and comparing the probability of any given site being consistent with and without erosion shows improvement (0.47±0.10 vs 0.37±0.10, respectively), but not significantly so within 1σ uncertainty. One could argue that calculating production rates over a range of erosion rates will naturally increase site by site uncertainties and hence result in better overall agreement amongst sites. Conversely though, including erosion is a realistic, and hence non-arbitrary way to increase site uncertainties and note that not all sites are affected to the same degree by the inclusion of erosion, so it is not strictly an all or none problem (Figure 2). The improvement is also borne out on a site-by-site basis (Figure 6, S3) where fewer sites have virtually zero probability of being consistent when erosion is incorporated into our analysis. The tradeoff between being near the average value regardless of uncertainty is well expressed. Sites with large uncertainties, but not larger than the value for an inconsistent Gaussian, can have rather high probabilities of being correct. The converse can also be true of a site, either because of tightly clustered ^{3}He measurements and/or precise age control, might yield overall small uncertainties for the site ^{3}He production rate, yet it is highly discrepant relative to the rest of the data. Thus, whereas an averaging approach such as the error weighted mean might be strongly biased by these precise calibration sites, the Press method is less strongly influenced.

All further discussion from this point forward refers to global reference ^{3}He production rates that account for the influence of erosion with uncertainties reported at the 1σ level. Direct comparison of our results (Table 1) with those of past ^{3}He production rate compilations and computation of a global reference production rate (Borchers et al., 2016; Delunel et al., 2016; Goehring et al., 2010; Lifton, 2016) is complicated by the fact that past studies have used different scaling schemes and/or not reported all models. When the same scaling models were used, most often Lal/Stone (Lal, 1991; Stone, 2000), different methods of air pressure calculation were employed, while differing geomagnetic models for cutoff rigidity calculations were used for time-dependent scaling models. Regardless, we note that our results, recalling that we account for a distribution of erosion rates for every site, are broadly like those of past studies when the Lal/Stone model is used for the purposes of comparison. What is more striking however, is that contrary to almost all previous studies which applied some method of subjective rejection of certain calibration sites, we apply an objective approach using the Press method to combine all calibration sites into a single reference production rate. Our approach yields a reference Lal/Stone production rate of 118±2.1 atoms g^{-1} yr^{-1}, similar to the most recent compilations (Delunel et al., 2016; Lifton, 2016; Martin et al., 2017) comprising a smaller global data sets. Most importantly, overall uncertainties on our reference ^{3}He production rates are lower than, or similar (Martin et al., 2017) to, those reported by previous compilations, even though we have included all datasets. We argue that this is largely a result of the use of the Press method for the averaging of individual site results, but also based on our reduction in scatter of site production rates across a range of ages because of the incorporation of site erosion.

It is important to note that we used ^{3}He concentrations as reported in their original publication. We made no corrections for ^{4}He in-growth due to U-Th-Sm decay, nor made corrections for production via thermal neutron capture on ^{6}Li. In some studies, these corrections are applied to the reported ^{3}He concentrations and are thus used (e.g., Amidon, 2011; Delunel et al., 2016). The former correction has been shown to possibly affect results up to 4% (Blard and Farley, 2008; Delunel et al., 2016), while the latter is only of consequence typically in pyroxene-bearing rocks, and is also small in magnitude (commonly $<0.02 \times 10^{6}$ atoms g^{-1}; Delunel et al., 2016). There is a possibility that exclusion of further ^{4}He and ^{6}Li corrections may introduce unintended bias in our results; however, we doubt that any bias introduced is greater than the magnitude of scatter observed (Table S1) nor the magnitude of the overall uncertainty on the reference global production rate.

Consideration of the non-spallogenic production mechanisms of ^3He and ^4He does however raise an interesting question regarding differences in production rates between olivine and pyroxene. Theoretical estimates of ^3He production in the two minerals phases have long suggested that there are significant differences (Masarik, 2002; Masarik and Beer, 1999; Masarik and Reedy, 1995). Additionally, Goehring et al. (2010) showed that there were differences in the absolute magnitude of production, but the differences were smaller than resulting uncertainties. Since then, additional sites studying both olivine and pyroxene production have emerged (Amidon, 2011; Eaves et al., 2015; Fenton et al., 2013; Foeken et al., 2012) that could yield insight into any mineralogical dependence. The dataset comprising our calibration effort is dominated by sites with olivine (n=36), compared to pyroxene (n=13) and yields a global reference production rate for olivine of 118±2.6 atoms g^{-1} yr^{-1} and 134±6.1 atoms g^{-1} yr^{-1} for pyroxene (both St scaling). The observed difference between olivine and pyroxene agrees with theoretical estimates (Masarik, 2002; Masarik and Reedy, 1995) in terms of sense of difference (pyroxene, 119 atoms g^{-1} yr^{-1}) > olivine, 115 atoms g^{-1} yr^{-1}), but not in terms of magnitude. Our results when incorporating erosion have a larger difference than theoretical results, as well as those of past compilations. While, in the absence of erosion our Bayesian approach yields a global reference ^3He pyroxene production rate similar to past estimates.

A set of questions naturally arises as to the correctness of our pyroxene global reference production rate. The pyroxene dataset is small relative to olivine and so during averaging of the pyroxene dataset, results could be dominated by tight clustering of data that are not necessarily representative of the actual pyroxene production rate particularly when incorporating erosion and its more pronounced effects on older sites. Figure 4 shows that relative to olivine, incorporation of erosion into the determination of the reference production rate has a greater impact when applying the Press method. We find it unlikely that most pyroxene sites have incorrect independent age determinations and do not consider further. Thus, three possibilities remain. 1) The pyroxene reference production rate is indeed higher than previously thought when sensible constraints on erosion are incorporated. We note that our dataset is larger than those previously used because additional datasets became available and our inclusion of all data in determining a reference global value may yield results different from previously presented. 2) The Press method fails to work properly in this case because of the relatively small number of pyroxene production rate calibrations sites. Examination of other methods for averaging (arithmetic mean and median) show similarly high (> 130 atoms g^{-1} yr^{-1}) values for pyroxene production. Only the inverse-error-weighted mean yields a value more in line with that of olivine, but this is likely the result of bias from highly precise data at lower production rates that are deemphasized by the Press analysis. 3) Constraints on erosion in the form of the prior are not appropriate for the pyroxene calibration sites available. We note that many of them are from relatively arid environments and thus erosion may be overestimated, which would lead to an overestimate of the ^{3}He production rate. The study of Amidon et al. (2011) does provide some guidance with regards to this possibility. The site age (18.2 ka; robustly tied to the catastrophic drainage of Lake Bonneville) is relatively young, and thus relatively unaffected by erosion compared to the older pyroxene calibration sites and yields a site reference production rate of 125±4.1 atoms g^{-1} yr^{-1} (LSDn), significantly less than the Press derived global value (Table 1). However, we also note that only four of the thirteen calibration sites yield reference production rates < 130 atoms g^{-1} yr^{-1} and only two of those less than 120 atoms g^{-1} yr^{-1}, therefore the bulk of the data indicates higher pyroxene ^{3}He production rates from sites spanning a range of ages.

One other potential issue arises from differences in corrections for nucleogenic production of ^{3}He from ^{6}Li. Pyroxene in general is high in both Li and thermal neutron sources such as U and

Th, relative to olivine, and thus correcting the cosmogenic ^3He component for Li-derived ^3He can be important. Most of the recent studies incorporate or assess these corrections and the corrected values have been used here (Amidon, 2011; Delunel et al., 2016; Foeken et al., 2012), yet high ^3He production rates persist. Repeat measurement of ^3He-bearing pyroxene intercomparison material (Blard et al., 2014; Schaefer et al., 2016; Muzikar et al., 2017) indicates that some laboratories yield systematically lower (or conversely, systematically higher) ^3He concentrations than others. No assessment of the potential influence of interlaboratory differences can be made on the older studies (Ackert et al., 2003; Cerling and Craig, 1994), but in general note that Blard et al. (2014) did observe a bimodal distribution amongst six labs for the ^3He bearing intercomparison material, so possible interlaboratory effects need further investigation.

At present, we cannot conclusively say whether the pyroxene ^3He production rate is higher than previously determined, or if other factors are influencing our results, but the suggestion of significantly higher ^3He production in pyroxene relative to olivine is present. Additional measurements by multiple laboratories from pyroxene-bearing calibration sites, particularly from relatively young sites where erosion can largely be ruled out, will be necessary before conclusive statements can be made.

6. Conclusions

Although cosmogenic nuclide production rate calibration studies always work to constrain a site's age and erosional history to the maximum extent possible, there will always remain some level of uncertainty. The ^3He production rate calibration dataset presented here evidences this, with some sites yielding anomalously low reference ^3He production rates (Figure 1). One possible explanation for this is that unaccounted-for site erosion may affect the inferred ^3He production rate. Here, we present a Bayesian approach to cosmogenic nuclide production rate calibration that allows for a researcher to account for a range of site erosion rates and ages, and incorporate information on the likelihood of a given erosion rate or age in the form of a prior probability distribution. Using an alternative averaging scheme where no sites are excluded a priori to determine the global reference sea level high latitude production rate yields values of 118±2 atoms g^{-1} yr^{-1} for olivine and pyroxene combined with the Lal/Stone scaling scheme. Similarly, for the LSDn model, we determined a value of 121±2 atoms g^{-1} yr^{-1}. We also observe differences in production between olivine and pyroxene, similar to that predicted by theoretical estimates, however with larger than predicted differences. The small number of calibration sites for pyroxene do not allow for robust conclusions to be made regarding this mineralogical difference and we encourage the development of more production rate calibration sites with pyroxene. Finally, we emphasize that our Bayesian approach to production rate calibration is widely applicable to the other cosmogenic nuclides, and could prove particularly useful for ^{14}C and ^{36}Cl with their sensitivity to secular equilibrium and multiple production pathways, respectively.

Acknowledgements

BMG acknowledges partial support from a NOAA Climate and Global Change Postdoctoral Fellowship and National Science Foundation award number EAR-1153689. PM and NAL acknowledge support from EAR-1560658. This manuscript and work was improved by fruitful conversations with Darryl Granger, Marc Caffee, Tibor Dunai, and Joerg Schaefer. We thank Mark Kurz for a thoughtful and helpful review.

References

Ackert Jr, R.P., Singer, B., Guillou, H., Kaplan, M., Kurz, M., 2003. Long-term cosmogenic 3He production rates from $^{40}Ar/^{39}Ar$ and K–Ar dated Patagonian lava flows at 47°S. Earth Planet. Sci. Lett. 210, 119-136.

Amidon, W., Farley, K., 2011. Cosmogenic ^{3}He production rate in apatite, zircon, and pyroxene inferred from Bonneville flood erosional surfaces. Quaternary Geochronology. 6, 10-21.

Balco, G., Briner, J., Finkel, R.C., Rayburn, J.A., Ridge, J.C., Schaefer, J.M., 2009. Regional beryllium-10 production rate calibration for late-glacial northeastern North America. Quaternary Geochronology. 4, 93-107.

Benson, L.V., Currey, D.R., Dorn, R.I., Lajoie, K.R., Oviatt, C.G., Robinson, S.W., Smith, G.I., Stine, S., 1990. Chronology of expansion and contraction of four Great Basin lake systems during the past 35,000 years. Palaeogeography, Palaeoclimatology, Palaeoecology 78, 241-286.

Bevington, P.R., Robinson, D.K., 2003. Data Reduction and Error Analysis for the Physical Sciences, 3rd ed. McGraw-Hill, New York.

Blard, P.-H., Balco, G., Burnard, P.G., Farley, K.A., Fenton, C.R., Friedrich, R., Jull, A.J.T., Niedermann, S., Pik, R., Schaefer, J.M., Scott, E.M., Shuster, D.L., Stuart, F.M., Stute, M., Tibari, B., Winckler, G., Zimmermann, L., 2014. An inter-laboratory comparison of cosmogenic ^{3}He and radiogenic ^{4}He in the CRONUS-P pyroxene standard. Quaternary Geochronology. 26, 11-19.

Blard, P.-H., Lavé, J., Sylvestre, F., Placzek, C.J., Claude, C., Galy, V., Condom, T., Tibari, B., 2013. Cosmogenic ^{3}He production rate in the high tropical Andes (3800 m, 20°S): Implications for the local last glacial maximum. Earth Planet. Sci. Lett. 377-378, 1-16.

Blard, P.H., Farley, K.A., 2008. The influence of radiogenic ^{4}He on cosmogenic ^{3}He determinations in volcanic olivine and pyroxene. Earth Planet. Sci. Lett. 276, 20-29.

Borchers, B., Marrero, S., Balco, G., Caffee, M., Goehring, B., Lifton, N., Nishiizumi, K., Phillips, F., Schaefer, J., Stone, J., 2016. Geological calibration of spallation production rates in the CRONUS-Earth project. Quaternary Geochronology. 31, 188-198.

Bronk Ramsey, C., 2001. Development of the radiocarbon calibration program. Radiocarbon.

Cerling, T.E., 1990. Dating Geomorphologic Surfaces using Cosmogenic He-3 Dating. Quat. Res. 33, 148-156.

Cerling, T.E., Craig, H., 1994. Cosmogenic ^{3}He production rates fro 39°N to 46°N latitude, western USA and France. Geochim. Cosmochim. Acta 58, 249-255.

Delunel, R., Blard, P.-H., Martin, L.C.P., Nomade, S., Schlunegger, F., 2016. Long term low latitude and high elevation cosmogenic 3He production rate inferred from a 107 ka-old lava flow in northern Chile; 22°S-3400ma.s.l. Geochim. Cosmochim. Acta 184, 71-87.

Dunai, T.J., Dunai, T., Stuart, F.M., Stuart, F., Pik, R., Burnard, P., Burnard, P., Gayer, E., Gayer, E., 2007. Production of 3He in crustal rocks by cosmogenic thermal neutrons. Earth Planet. Sci. Lett. 258, 228-236.

Dunai, T.J., Wijbrans, J.R., 2000. Long-term cosmogenic ^{3}He production rates (152 ka-1.35 Ma) from ^{40}Ar/^{39}Ar dated basalt flows at 29°N latitude. Earth Planet. Sci. Lett. 176, 147-156.

Eaves, S.R., Winckler, G., Schaefer, J.M., Vandergoes, M.J., Alloway, B.V., Mackintosh, A.N., Townsend, D.B., Ryan, M.T., Xun, L., 2015. A test of the cosmogenic ^{3}He production rate in the south-west Pacific (39°S). J. Quat. Sci. 30, 79-87.

Fenton, C.R., Mark, D.F., Barfod, D.N., Niedermann, S., Goethals, M.M., Stuart, F.M., 2013. ^{40}Ar/^{39}Ar dating of the SP and Bar Ten lava flows AZ, USA: Laying the foundation for the SPICE cosmogenic nuclide production-rate calibration project. Quat. Geochron. 18, 158-172.

Foeken, J.P.T., Stuart, F.M., Mark, D.F., 2012. Long-term low latitude cosmogenic ^{3}He production rate determined from a 126 ka basalt from Fogo, Cape Verdes. Earth Planet. Sci. Lett. 359-360, 14-25.

Goehring, B.M., Kurz, M.D., Balco, G., Schaefer, J.M., Licciardi, J., Lifton, N., 2010. A reevaluation of in situ cosmogenic ^{3}He production rates. Quat. Geochron. 5, 410-418.

Kelly, M. A., Lowell, T. V., Applegate, P. J., Phillips, F. M., Schaefer, J. M., Smith, C. A., et al. 2015. A locally calibrated, late glacial 10 Be production rate from a low-latitude, high-altitude site in the Peruvian Andes. Quaternary Geochronology. 26, 70–85. http://doi.org/10.1016/j.quageo.2013.10.007

Kurz, M.D., 1986. In situ production of terrestrial cosmogenic helium and some applications to geochronology. Geochim. Cosmochim. Acta 50, 2855-2862.

Kurz, M.D., Colodner, D., Trull, T.W., Moore, R.B., O'Brien, K., 1990. Cosmic ray exposure dating with in situ produced cosmogenic 3He: results from young Hawaiian lava flows. Earth Planet. Sci. Lett. 97, 177-189.

Lal, D., 1991. Cosmic ray labeling of erosion surfaces: *in situ* nuclide production rates and erosion models. Earth Planet. Sci. Lett. 104, 424-439.

Licciardi, J.M., Kurz, M.D., Clark, P.U., Brook, E.J., 1999. Calibration of cosmogenic ^{3}He production rates from Holocene lava flows in Oregon, USA, and effects of the Earth's magnetic field. Earth Planet. Sci. Lett. 172, 261-271.

Lifton, N., 2016. Implications of two Holocene time-dependent geomagnetic models for cosmogenic nuclide production rate scaling. Earth Planet. Sci. Lett. 433, 257-268.

Marrero, S.M., Phillips, F.M., Borchers, B., Lifton, N., Aumer, R., Balco, G., 2016. Cosmogenic nuclide systematics and the CRONUScalc program. Quat. Geochron. 31, 160-187.

Martin, L.C.P., Blard, P.H., Balco, G., Lavé, J., Delunel, R., Lifton, N., Laurent, V., 2017. The CREp program and the ICE-D production rate calibration database: A fully parameterizable and updated online tool to compute cosmic-ray exposure ages. Quat. Geochron. 38, 25-49.

Masarik, J., 2002. Numerical simulation of in-situ production of cosmogenic nuclides. Geochim. Cosmochim. Acta 66, A491-A491.

Masarik, J., Beer, J., 1999. Simulation of particle fluxes and cosmogenic nuclide production in the Earth's atmosphere. Journal of Geophys. Res. 104, 12099-12111.

Masarik, J., Reedy, R.C., 1995. Terrestrial cosmogenic-nuclide production systematics calculated from numerical simulations. Earth Planet. Sci. Lett. 136, 381-395.

McGee, D., Quade, J., Edwards, R.L., Broecker, W.S., Cheng, H., Reiners, P.W., Evenson, N., 2012. Lacustrine cave carbonates: Novel archives of paleohydrologic change in the Bonneville Basin (Utah, USA). Earth Planet. Sci. Lett. 351–352, 182-194.

Muzikar, P., Goehring, B.M., Lifton, N., 2017. Handling overdispersion in CRONUS-Earth intercomparison measurements: a Bayesian approach. Radiocarbon 58, 1133-1145.

Oviatt, C.G., Currey, D.R., Sack, D., 1992. Radiocarbon Chronology of Lake Bonneville, eastern Great Basin, USA. Palaeogeography Palaeoclimatology Palaeoecology 99, 225-241.

Oviatt, C.G., Nash, W.P., 1989. Late Pleistocene Basaltic Ash and Volcanic-Eruptions in the Bonneville Basin, Utah. Geol Soc America Bull 101, 292-303.

Pavón-Carrasco, F.J., Osete, M.L., Torta, J.M., De Santis, A., 2014. A geomagnetic field model for the Holocene based on archaeomagnetic and lava flow data. Earth Planet. Sci. Lett. 388, 98-109.

Phillips, F.M., Argento, D.C., Balco, G., Caffee, M.W., Clem, J., Dunai, T.J., Finkel, R., Goehring, B., Gosse, J.C., Hudson, A.M., Jull, A.J.T., Kelly, M.A., Kurz, M., Lal, D., Lifton, N., Marrero, S.M., Nishiizumi, K., Reedy, R.C., Schaefer, J., Stone, J.O.H., Swanson, T., Zreda, M.G., 2016a. The CRONUS-Earth Project: A synthesis. Quat. Geochron. 31, 119-154.

Phillips, F. M., Argento, D. C., Bourlès, D. L., Caffee, M. W., Dunai, T. J., Goehring, B. M., et al. 2016b. Where now? Reflections on future directions for cosmogenic nuclide research from the CRONUS Projects. Quaternary Geochronology. 31, 155–159.

Portenga, E.W., Bierman, P.R., 2011. Understanding Earth's eroding surface with 10Be. GSA Today 21, 4-10.

Press, W., 1997. Understanding data better with Bayesian and global statistical methods, in Unsolved Problems in Astrophysics, in: Bachall, J.N., Ostriker, J.P. (Eds.), Unsolved Problems in Astrophysics. Princeton University Press, pp. 49-60.

Schaefer, J.M., Winckler, G., Blard, P.-H., Balco, G., 2016. Performance of CRONUS-P–a pyroxene reference material for helium isotope analysis. Quaternary Geochronology. 31, 237-239.

Stone, J.O., 2000. Air pressure and cosmogenic isotope production. Journal of Geophysical Research 105, 23753-23759.

Tables

Table 1. Summary of global production rate (^3He atoms g^{-1} yr^{-1}) calibration results with erosion of 0-5 m Myr^{-1} using multiple methods to establish central tendency values. Uncertainties are reported at the 1σ-level. Description of the Press method for averaging is described in methods section (Muzikar et al., in review; Press, 1997). For the error weighted mean, the uncertainty is taken as the larger of the uncertainty in weighted mean or the weighted average variance (Bevington and Robinson, 2003). Uncertainty on the median is based on the half-width of the interquartile range.

	Press ± 1σ	Mean ± 1σ	EWM ± 1σ (std error)	X_v^2	Median ± IQR
Lal/Stone					
Olivine + Pyroxene (n=49)	119±2.2	127±28	120±0.84	13.42	123±18
Olivine (n=36)	118±2.6	126±31	120±0.99	14.26	121±19
Pyroxene (n=13)	134±6.1	130±22	118±1.6	11.99	131±13
LSDn					
Olivine + Pyroxene (n=49)	121±2.1	139±27	137±0.82	33.18	135±20
Olivine (n=36)	119±1.6	139±29	140±0.91	38.83	128±21
Pyroxene (n=13)	145±9.8	139±23	126±1.8	15.79	138±16

Figures

Figure 1. Reference ^{3}He production rates for all sites used in our analysis shown versus site age, site latitude, and site elevation. Production rates were calculated assuming zero erosion and are shown by mineral phase analyzed following the methods presented here. Reference production rates are shown for the nuclide specific scaling model of Lifton et al. (2014) (aka LSDn) and the time dependent geomagnetic framework of Lifton (2016). For simplicity we refer to them both hence forth as LSDn.

Figure 2. Plot of the sensitivity of apparent ^{3}He production rate for a range of erosion rates and ages. Contours show the percent underestimation the calculated production rate is relative to the true production rate. Here we assumed a ^{3}He production rate of 120 at g^{-1} yr^{-1} as the true production rate.

Figure 3. Resulting reference ^{3}He production rate posterior distributions for three representative sites included in the current study. Sites selection is based on their age and method of age control displaying the effects of various forms of the prior for erosion and or site age. For example, Tabernacle Hill (top panel) is relatively young (ca. 18 ka) and therefore little affected by erosion (Lifton et al., 2015 estimated less than a few millimeters of total erosion), has a uniform prior probability for its age and therefore results in a flat-topped posterior. Yapoah Crater is even younger (~ 2 ka) and therefore is virtually unaffected by erosion, but because of its age control resulting from radiocarbon dating, displays a non-Gaussian posterior reflecting the shape of the calibrated radiocarbon age PDF. Finally, SP Flow is relatively old (~72 ka) and therefore is more strongly affected by the range of erosion over which we integrate and by the form of the prior for erosion, as reflected by lower probability at higher production rates (i.e., where less-likely but higher erosion rates would lead to higher apparent production rates).

Figure 4. Probability distributions for the global reference LSDn ^{3}He production rate as derived from the Press approach. Results are shown for olivine and pyroxene separately, as well as combined. The combined mineral phases global production rate is strongly influenced by the much larger olivine dataset compared to the pyroxene dataset. Top, case of integrating over 0-5 m Myr^{-1}; bottom, case of zero erosion.

Figure 5. Sensitivity analysis of resulting summary reference ^{3}He production rate to our choice of S, or the size of bad Gaussian, in the Press approach. In our analysis, S is chosen to minimize its effect on the resulting production rate. Values greater than 20 atoms g^{-1} yr^{-1} for s result in little change to the resulting average value. We have thus taken an approach that aims to include more data and purposefully chosen the value for the width of bad Gaussian to wide at five times the arithmetic mean of the site production rate uncertainties. Shaded region shows range of resulting production rates at 1σ.

Figure 6. Probability that each site reference ^{3}He production rate is consistent for both the no-erosion (top) and range of erosion rate cases (bottom). Probabilities of consistency are plotted against the site production rate. Error bars are shown at the 1σ level. While the distribution of site production rates is skewed slightly higher for the erosion case, overall probabilities of consistency are increased.

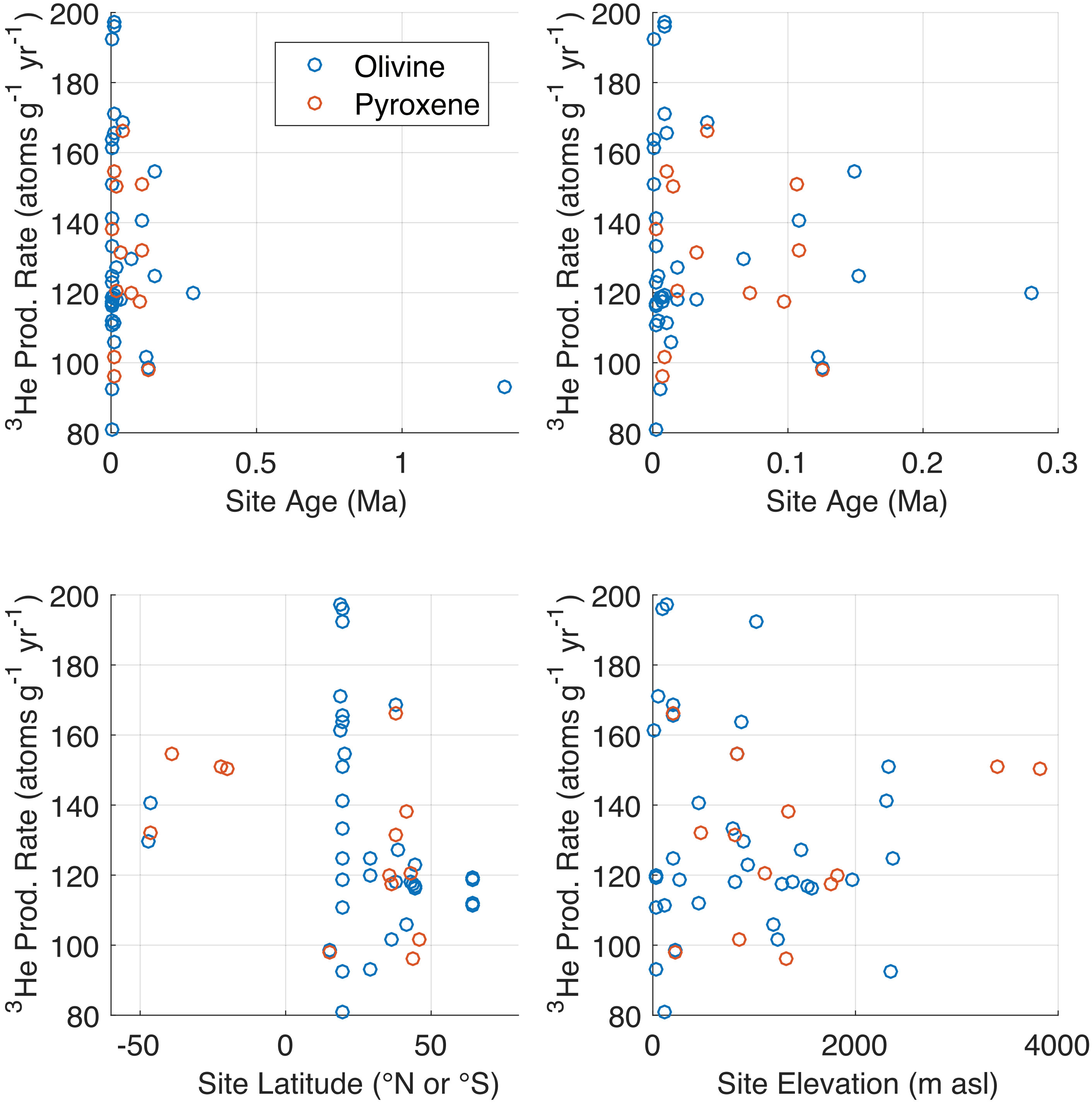

Goehring Figure 1

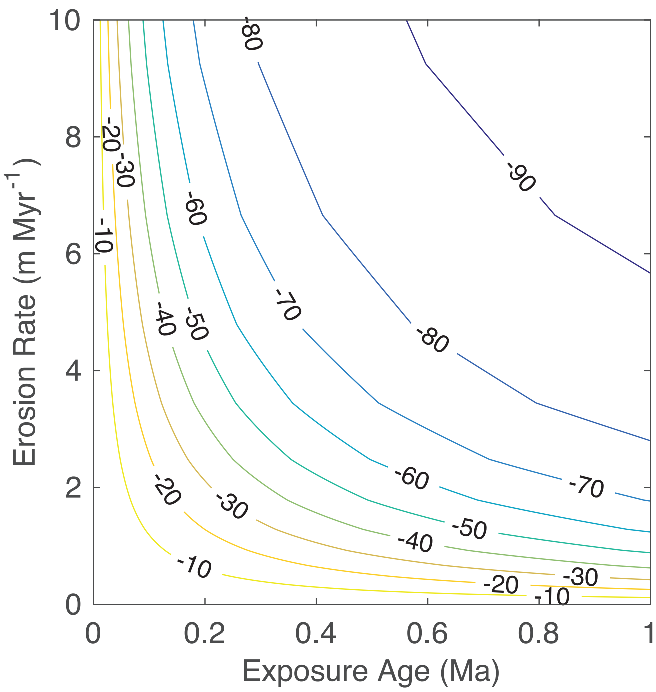

Goehring Figure 2

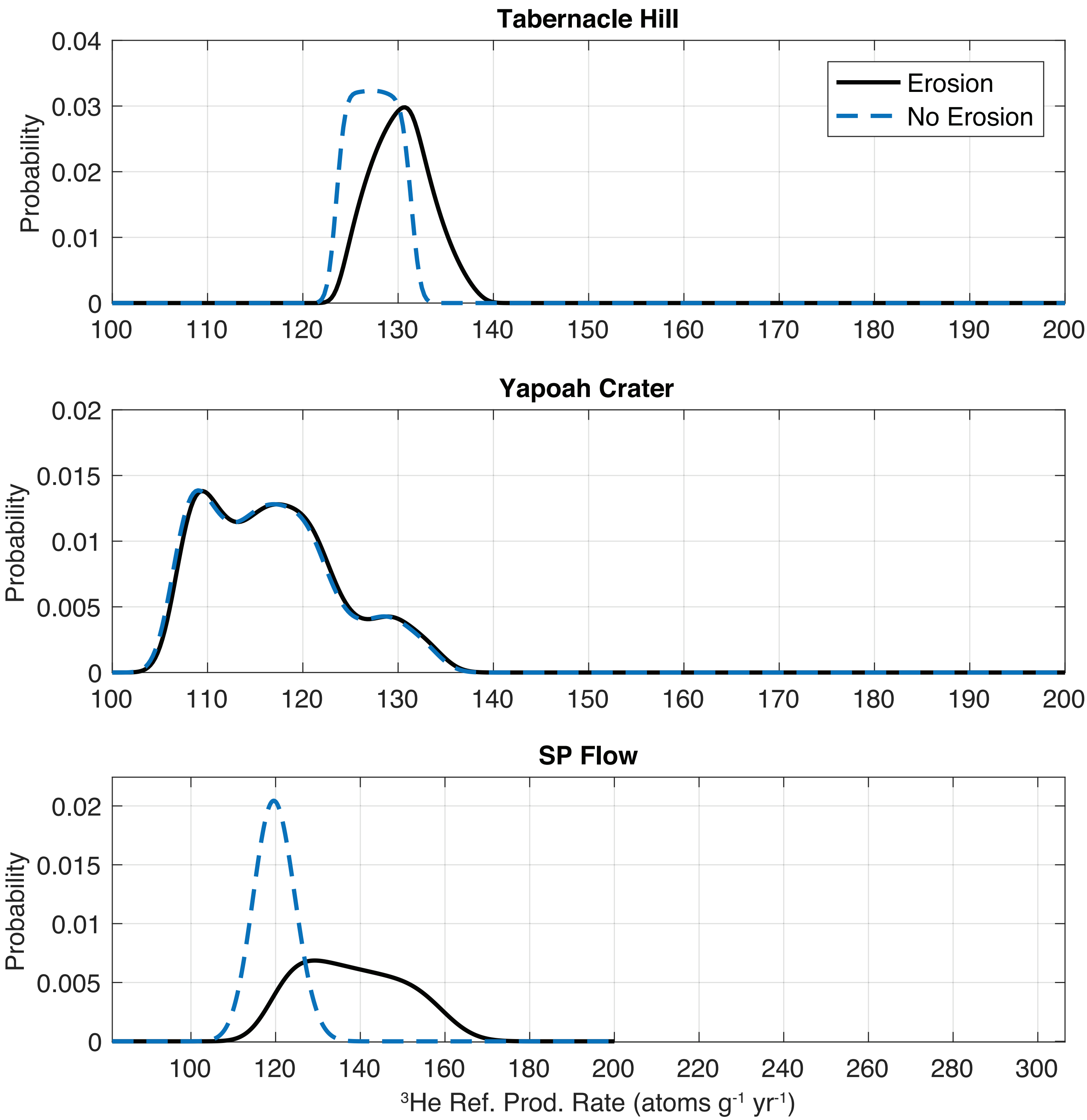

Goehring Figure 3

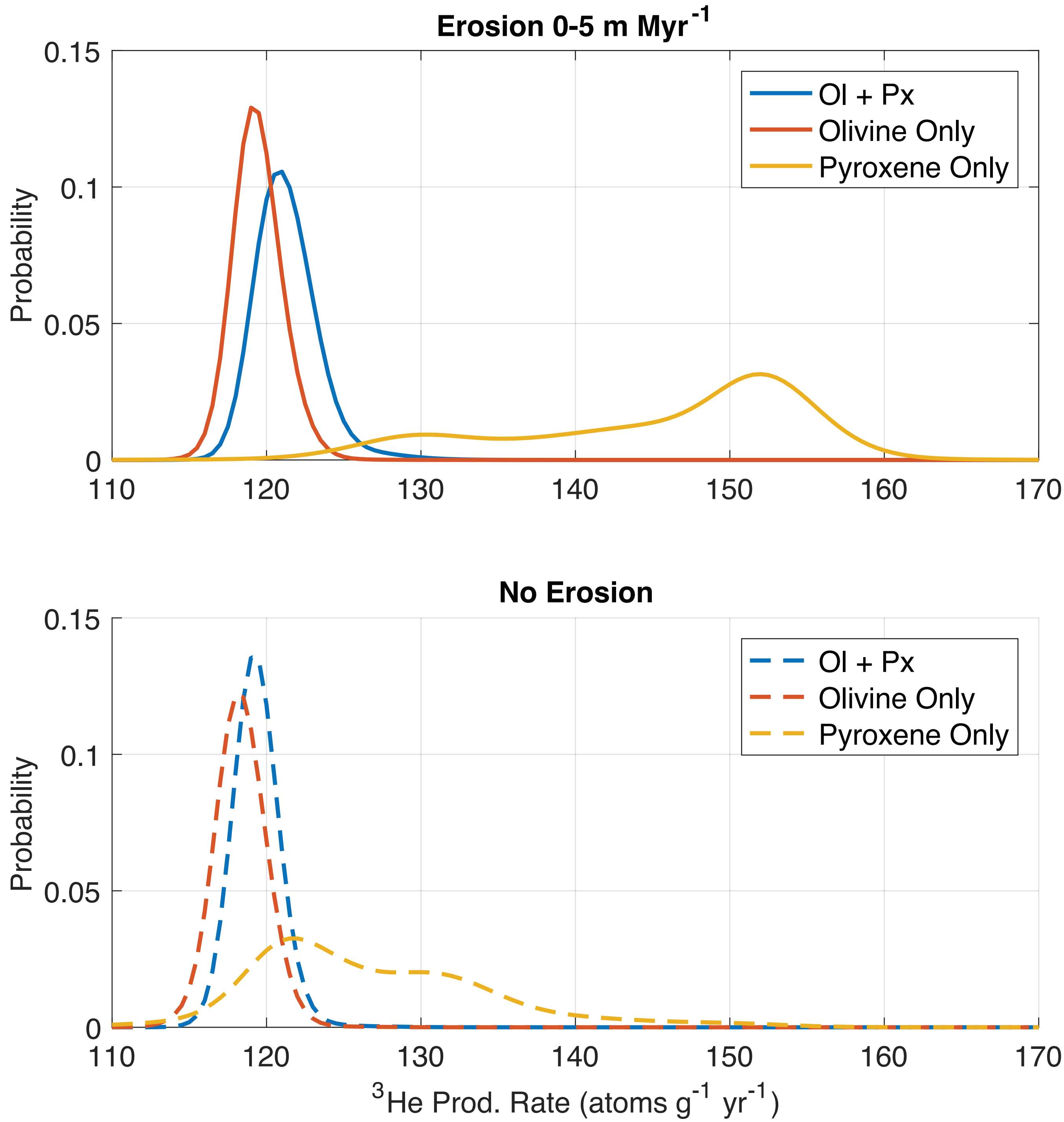

Goehring Figure 4

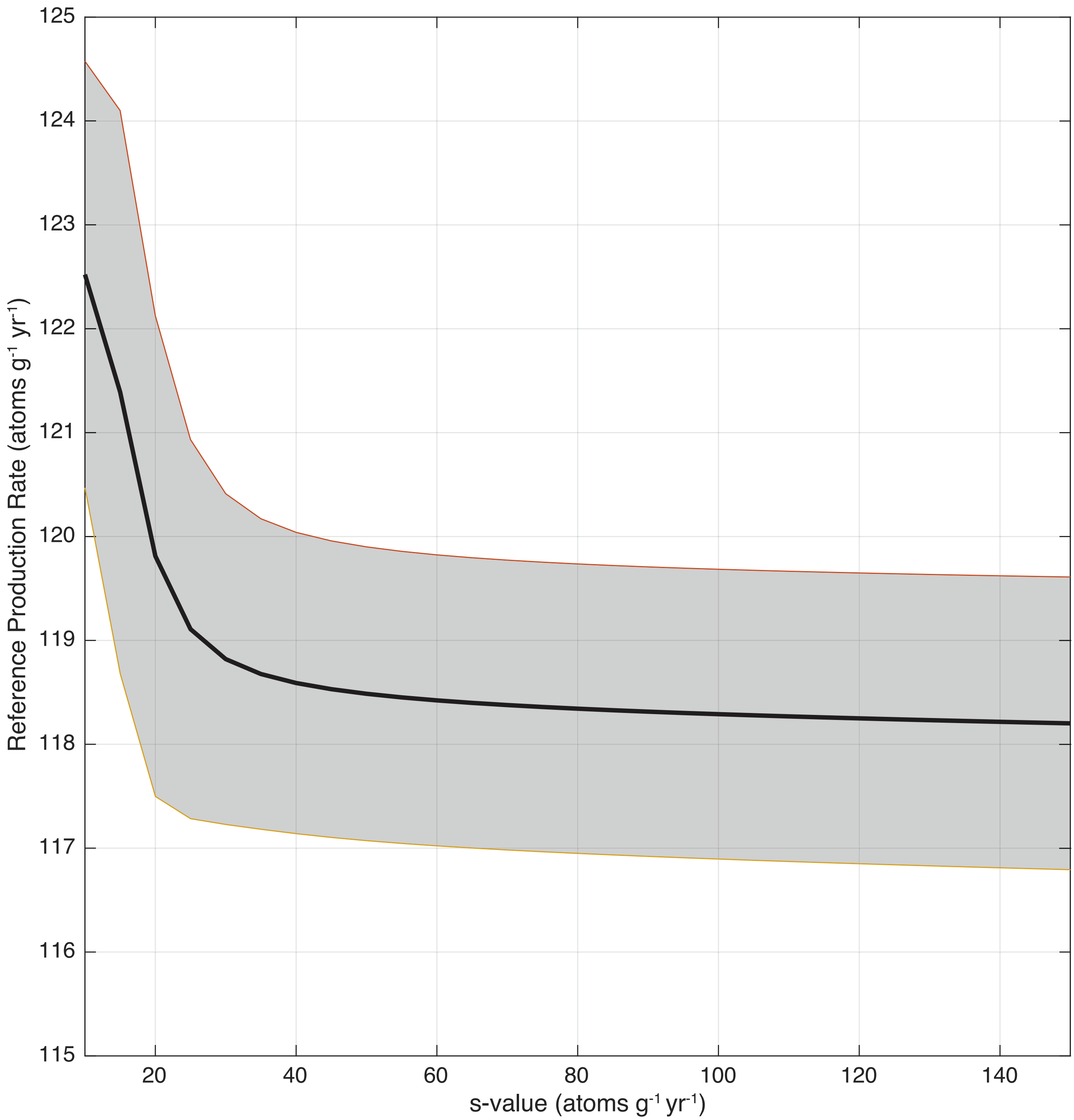

Goehring Figure 5

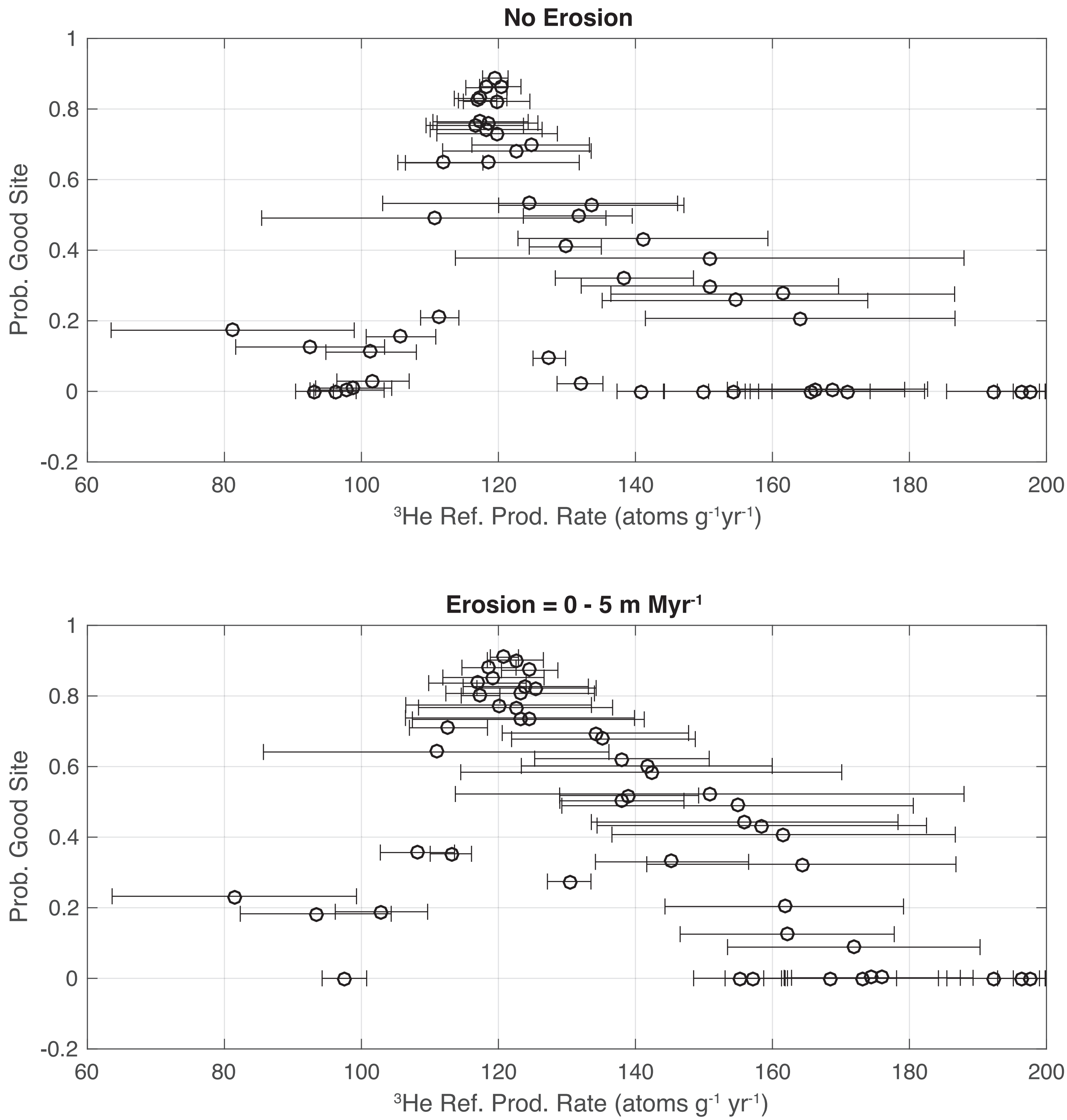

Goehring Figure 6 rev